Published in final edited form as:
Mol Cancer Ther. 2007 November ; 6(11): 2879–2890. doi:10.1158/1535-7163.MCT-07-0297.

Collaboration between Hepatic and Intratumoral Prodrug Activation in a P450 Prodrug-activation Gene Therapy Model for Cancer Treatment

Jie Ma and **David J. Waxman**
Division of Cell and Molecular Biology, Department of Biology, Boston University, 5 Cummington Street, Boston, MA 02215

Abstract

Presently, we investigate the mechanisms whereby intratumoral expression of a cyclophosphamide (CPA)-activating hepatic cytochrome P450 gene enhances therapeutic activity when CPA is given on an every 6-day (metronomic) schedule. In P450-deficient 9L gliosarcomas grown in *scid* mice, metronomic CPA substantially decreased tumor microvessel density and induced a ~70% loss of endothelial cells that began after the second CPA treatment. These responses were accompanied by increased expression of the endogenous angiogenesis inhibitor thrombospondin-1 in tumor-associated host cells but by decreased expression in 9L tumor cells. These anti-angiogenic responses preceded tumor regression and are likely key to the therapeutic activity of metronomic CPA. Unexpectedly, 9L/2B11 tumors, grown from 9L cells infected with retrovirus encoding the CPA-activating P450 2B11, exhibited anti-angiogenic responses very similar to 9L tumors. This indicates that the tumor endothelial cell population is well exposed to liver-activated CPA metabolites and that intratumoral P450 confers limited additional anti-endothelial cell bystander activity. In contrast, TUNEL assay revealed an increase in apoptosis that preceded the anti-angiogenic response and was substantially enhanced by intratumoral P450 2B11 expression. 9L/2B11 tumor regression was accompanied by an overall loss of tumor cellularity and by substantial enlargement of remaining P450-immunoreactive tumor cells as the number of P450-positive tumor cell decreased and the P450 protein content declined with CPA treatment. We conclude that metronomic CPA regresses P450-expressing tumors by two independent but complementary mechanisms: increased tumor cell killing *via* intratumoral P450-catalyzed prodrug activation, coupled with strong anti-angiogenic activity, which is primarily associated with hepatic prodrug activation.

Keywords

Cyclophosphamide; Anti-angiogenesis; Gene-Directed Enzyme-Prodrug Therapy

INTRODUCTION

Cancer chemotherapeutic drugs are often administered at their maximum tolerated doses (MTD) to maximize the killing of malignant cells; however, the effectiveness of this approach is limited by the collateral damage to proliferating cells in the intestinal epithelium, bone marrow, and hair follicles. Strategies to improve tumor cell-specific targeting include the use of antibody- or aptamer-cytotoxin conjugates (1,2), antibody-directed immunoliposomes (3), and systemic delivery of anti-cancer prodrugs in combination with tumor-specific expression

CORRESPONDING AUTHOR David J. Waxman, Department of Biology, Boston University, 5 Cummington Street, Boston, MA 02215, Tel: 617-353-7401, Fax: 617-353-7404, email: djw@bu.edu.

of prodrug-activating enzymes. This latter approach, termed gene-directed enzyme-prodrug therapy (GDEPT), has been studied with a variety of enzyme-prodrug combinations, including cytochrome P450 with the oxazaphosphorine alkylating agent prodrug cyclophosphamide (CPA). The development of GDEPT strategies combining P450 enzymes with CPA has been facilitated by the extensive clinical experience with CPA, the diffusibility of its active 4-hydroxy metabolite, and the associated bystander cytotoxic effect. P450-based GDEPT has been exemplified in preclinical studies using vectors based on retrovirus (4), herpes virus (5) and adenovirus (6), and by using encapsulated cells engineered to express cytochrome P450 (7). P450-based GDEPT substantially improves anti-tumor activity in preclinical studies and initial clinical trials have been positive (8,9).

Much progress has been made since angiogenesis was first proposed as a target for cancer therapy (10), with several anti-angiogenic agents now in clinical use (11). When administered at a low dose but at frequent intervals (i.e., a metronomic schedule), CPA and several other traditional chemotherapeutic drugs show anti-angiogenic activity and inhibit tumor growth in xenograft models, whereas the same drug given at a similar total dose but using a MTD regimen is much less effective (12–16). In clinical trials, daily low dose CPA given in combination with other chemotherapeutic drugs provides clinical benefit with minimal toxicity to patients with advanced solid tumors (17,18). Traditional chemotherapeutics administered on a metronomic schedule may find use as cost effective alternatives to new and expensive anti-angiogenic drugs now in development (19).

Compared to an MTD regimen, metronomic CPA shows substantially enhanced anti-tumor activity in the rat 9L gliosarcoma model (13,20), however, the role of tumor cell cytotoxicity vs. anti-angiogenesis in the observed therapeutic response is unclear. Introduction of a prodrug-activating P450 gene into tumor cells accelerates tumor regression and extends the tumor-free period following metronomic CPA treatment (20), but it is not known how P450-catalyzed intratumoral drug activation affects the anti-angiogenic response. In particular, it is unclear whether the therapeutic activity of P450-based GDEPT primarily results from an increase in direct tumor cell killing, or whether the localized production of active drug metabolites enhances the anti-angiogenic response. To address these issues, we presently investigate the changes in tumor vascularization and apoptosis in a tumor xenograft model expressing P450 2B11, a highly efficient catalyst of CPA activation characterized by an atypically low K_m (21). We also study the impact of metronomic CPA treatment on the expression of the CPA-activating P450 enzyme. Our findings demonstrate that P450-based GDEPT enhances anti-tumor activity primarily by chemosensitizing tumor cells, without changing activity against tumor-associated endothelial cells. Overall anti-tumor activity is thus optimized when P450 gene delivery is combined with tumor endothelial cell-directed metronomic CPA treatment.

MATERIALS AND METHODS

Chemicals and Antibodies

CPA (C0768), collagenase type IV (C5138), DNase I (D5025), and mouse monoclonal anti-smooth muscle actin-α antibody (A5228) were purchased from Sigma-Aldrich Co. (St. Louis, MO). Fetal bovine serum (FBS), D-MEM medium, and TRIzol reagent were purchased from Invitrogen (Carlsbad, CA). 16% paraformaldehyde solution (methanol-free) was purchased from Electron Microscopy Sciences (Hatfield, PA). FITC-conjugated (553372) or unconjugated (557355) rat monoclonal anti-CD31 antibody (IgG_{2a}), and FITC-conjugated rat IgG_{2a} (553929) were purchased from BD Bioscience (Franklin Lakes, NJ). Mouse monoclonal anti-TSP-1 antibody (MS-421; reactive with rat and mouse TSP-1) was purchased from Lab Vision Co. (Fremont, CA). Goat polyclonal anti-TSP-1 antibody (sc-12312; reactive with mouse TSP-1) was purchased from Santa Cruz Biotechnology (Santa Cruz, CA). Rabbit polyclonal anti-P450 2B11 antibody was a gift from Dr. James Halpert, University of Texas

Medical Branch (Galveston, TX). Mouse monoclonal anti-P450 2B6 antibody (A326) was purchased from BD Gentest (Woburn, MA). Horseradish peroxidase (HRP)-conjugated donkey-anti-rabbit antibody (NA934) was from Amersham Biosciences (Little Chalfont, United Kingdom). Normal horse serum, normal rabbit serum, avidin/biotin blocking kit, biotinylated secondary antibodies (horse-anti-mouse antibody BA-2000; rabbit-anti-goat antibody BA-5000; rabbit-anti-rat antibody BA-4000), Vectastain Elite ABC Kit, peroxidase substrates (3, 3'-diaminobenzidine, DAB; 3, 3', 5, 5'-tetramethylbenzidine, TMB; and VIP), VectaMount and Gill's Hematoxylin were from Vector Laboratories (Burlingame, CA). DeadEnd™ Colorimetric TUNEL kit and RNase-free DNase (M6101) were from Promega (Madison, WI). 1% alcoholic eosin Y was purchased from Fisher Scientific (Hampton, NH). Random hexamers (N808-0127), MuLV reverse transcriptase (N808-0018), RNase inhibitor (N808-0119), and SYBR Green PCR Master Mix (#4309155) were purchased from Applied Biosystems (Foster City, CA). D_c Protein Assay kit was purchased from Bio-Rad (Hercules, CA). SuperSignal West Femto Maximum Sensitivity Substrate was purchased from Pierce Biotechnology (Rockford, IL).

Tumor Cell Lines

9L rat gliosarcoma cells infected with retrovirus encoding P450 reductase in combination with either P450 2B11 or P450 2B6 (9L/2B11 and 9L/2B6 cells, respectively) and 9L tumor cells infected with the empty retroviral vector pBabe (9L/pBabe cells, herein referred to as 9L cells) were described previously (20).

Tumor Growth Delay Experiments

Immune-deficient male Fox Chase ICR *scid* mice (Taconic Farms, Germantown, NY) were housed in the Boston University Laboratory Animal Care Facility in accordance with approved protocols and federal guidelines. Autoclaved cages containing food and water were changed weekly. Mouse body weight was monitored every 3 d. 9L, 9L/2B11 and 9L/2B6 cells used for tumor inoculation were grown in D-MEM containing 10% FBS, trypsinized, resuspended in FBS-free D-MEM at a concentration of 8×10^6 cells/ml, then kept on ice until injection. 4×10^6 cells in a volume of 0.5 ml were injected *s.c.* into each flank of a 5-wk-old *scid* mouse using a 27 gauge needle. Tumor sizes (length L × width W) were measured every 3 d using Vernier calipers (Manostat Co., Switzerland) and volumes (V) calculated from $V=(\pi/6)\times(L\times W)^{3/2}$. CPA treatment was initiated when the average tumor volume reached ~500 mm^3. Fresh CPA solution dissolved in PBS (140 mM NaCl, 10 mM Na_2HPO_4, 2.7 mM KCl, 1.8 mM KH_2PO_4) was filtered through a 0.2 μm Acrodisc syringe filter (Pall Co., Ann Arbor, MI) and administered to the tumor-bearing mice by *i.p.* injection at 140 mg CPA/kg body weight every 6 d (13).

Tumor Cryosectioning and Immunohistochemical Staining

Fresh tumor tissues were snap frozen in dry ice-cold 2-methylbutane and stored at −80°C. Tumor cryosections (6 μm, 3–4 sections/slide) were prepared using a Leica 1800 cryostat and fixed with 1% paraformaldehyde at room temperature for 30 min. Following a PBS wash, the sections were incubated with permeabilization solution containing 1% Triton X-100 (v/v) and 1% sodium citrate (w/v) for 5 min on ice followed by a second PBS wash. Sections were blocked at room temperature for 20 min with PBS containing 2% normal serum from the species in which the secondary antibody was raised, except for normal horse serum, which was used in place of normal donkey serum. The slides were then incubated with primary antibody for 1 h at 37°C followed by a PBS wash. The secondary antibody was also incubated for 1 h at 37° C followed by another PBS wash. The sections were then incubated with ABC complex for 30 min at room temperature. Peroxidase substrate (DAB, DAB-Nickel, TMB, or VIP) was added and color development was terminated by immersing the slides in tap water. After

hematoxylin counterstaining, the slides were dehydrated by sequential washing with 95% ethanol, 100% ethanol and 100% xylene and sealed with VectaMount. The final concentration of each primary antibody was as follows: CD31 (0.3 μg/ml), P450 2B6 (1:2000 dilution), P450 2B11 (8 μg/ml), smooth muscle actin-α (5 μg/ml), and TSP-1 (4 μg/ml for antibody MS-421; 2 μg/ml for antibody sc-12312). Secondary antibodies were diluted to 7.5 μg/ml (biotinylated anti-goat, anti-mouse, and anti-rat antibodies) or 1:500 (HRP-conjugated anti-rabbit antibody). Because of the different sensitivities of each primary antibody and peroxidase substrate, CD31/DAB staining was always carried out first when samples were double immunostained, followed by staining with anti-TSP-1 (sc-12312)/TMB or anti-smooth muscle actin-α/TMB. Avidin/biotin blocking kit was used for double immunostaining per the manufacturer's protocol.

Tumor Microvessel Density

CD31-stained tumor sections were examined using an Olympus BX50 bright-field light microscope. A representative section was identified for each tumor and the number of blood vessels was counted in five random fields per section at a magnification of 400x. Microvessel density was presented as mean ± SE for four individual tumors per treatment group at each time point.

Preparation of Single Cell Suspension from Fresh Tumor Tissue

Tumor-bearing mice were killed by cervical dislocation. Fresh tumor tissue (100–200 mg) was washed in ice-cold PBS, transferred to 10 ml of ice-cold D-MEM containing 10% FBS and cut into small pieces. The mixture was centrifuged at 300 g for 5 min at 4°C and the pellet was resuspended in 10 ml of D-MEM containing 4500 U/ml of collagenase IV and 0.1 mg/ml of DNase I. After initial digestion for 15 min at 37°C with vigorous shaking, an additional 1 ml of 4500 U/ml collagenase IV and 1 ml of 1 mg/ml DNase I were added under aseptic conditions followed by digestion for another 15 min. The solution was centrifuged at 700 g for 10 min at 4°C. The pellets were gently re-suspended in 10 ml of ice-cold D-MEM with 10% FBS. The cell suspension was filtered through a 70 μm cell strainer, which was rinsed with 10 ml of D-MEM containing 10% FBS. The filtered cell suspension was centrifuged at 700 g for 10 min at 4°C and the supernatant was carefully removed. The pellets were gently washed with 10 ml of ice-cold D-MEM containing 10% FBS and centrifuged again at 300 g for 5 min at 4°C. The final cell pellets were suspended in 0.3–1 ml of immunostaining buffer (IS buffer; PBS containing 2% FBS and 0.1% NaN_3). Cell viability was determined by trypan blue exclusion.

CD31 Immunostaining and Flow Cytometric Analysis

Individual tumors (n = 3–4/group) were analyzed at each CPA treatment time point. First, 2.5×10^5 cells were suspended in 0.1–0.2 ml of IS buffer and incubated with 0.25 μg of FITC-conjugated CD31 antibody or isotype control rat IgG_{2a} for 60 min at 4°C in the dark. After staining, the cells were washed with ice-cold IS buffer and centrifuged at 300 g for 5 min at 4°C. The pellets were resuspended in 500 μl of IS buffer and analyzed using a FACS Calibur flow cytometer (BD Bioscience, Franklin Lakes, NJ) and FlowJo software (Tree Star Inc., Ashland, OR) for data analysis. Total events (100,000–200,000) were counted during FACS analysis. Both the number of CD31-positive cells and the number of total cells were determined. The percentage of CD31-positive cells in the total tumor cell population was calculated and the data were expressed as mean ± SE for 3–4 individual tumors per group.

Hematoxylin-Eosin Staining

Cryosections were fixed in 4% formaldehyde for 15 min at room temperature, washed with PBS, stained in Gill's Hematoxylin for 2 min and then rinsed with tap water. Following 10 dips in 2% acetic acid and then 10 dips in 0.45% NH_4OH, the sections were stained in 1%

eosin Y and then dehydrated by sequential washings with 95% ethanol, 100% ethanol, 100% xylene and sealed with VectaMount.

TUNEL Assay

The TUNEL assay was performed according to the manufacturer's protocol (Promega) with modifications. Tumor cryosections were fixed in 4% paraformaldehyde at room temperature for 15 min. After washing with PBS, the sections were incubated with permeabilization solution containing 1% Triton X-100 (v/v) and 1% sodium citrate (w/v) for 10 min on ice. Following a PBS wash, the sections were fixed again with 4% paraformaldehyde for 5 min. After another PBS wash, the sections were incubated with equilibration buffer for 10 min and then incubated with biotinylated dNTPs and terminal deoxynucleotidyl transferase for 1 h at 37°C. Reactions were terminated by washing with 2×SSC buffer (300 mM NaCl, 35 mM sodium citrate) for 15 min. The sections were immersed in 0.3% H_2O_2 for 5 min to block endogenous peroxidase. After incubation with streptavidin HRP (1:500 diluted in PBS) for 30 min, VIP was used as the peroxidase substrate. Color development was terminated by rinsing the slides in tap water. After dehydration, the slides were sealed with VectaMount. The number of TUNEL-positive cells in the entire section was counted at 200x magnification and the average number of apoptotic cells per field (i.e., apoptotic index) was calculated and expressed as mean ± SE of four individual tumors.

Real-time PCR

TSP-1 and P450 2B11 RNA were quantified in 9L tumors by quantitative, real-time PCR (qPCR) using SYBR Green I chemistry. Fresh tissue samples were excised and snap-frozen in liquid nitrogen, then stored at −80°C. On the days of CPA administration, the samples were collected prior to CPA injection. Total RNA was isolated from frozen tissue samples (0.1–0.4 g) using TRIzol reagent according to the manufacturer's protocol. RNA (1 μg) was treated with DNase I for 60 min at 37°C to remove any DNA contamination. After heating for 10 min at 75°C to inactivate the DNase, cDNA was synthesized by reverse transcription in a 20 μl reaction containing random hexamers, MuLV reverse transcriptase and RNase inhibitor. A 4 μl portion of the final reaction was diluted 1:50 in 50 ng/μl yeast tRNA and used as template DNA for qPCR assays. Forward and reverse qPCR primers were as following: 18S rRNA, 5'-CGCCGCTAGAGGTGAAATTC-3' and 5'-CCAGTCGGCATCGTTTATGG-3'; mouse TSP-1, 5'-TGTTCAAGAGGACCGGGCT-3' and 5'-TGGATGGGTACATCCAGCTCC-3'; rat TSP-1, 5'-CCGGTTTGATCAGAGTGGT-3' and 5'-GGTTTCGGAAGGTGCAAT-3'; total (rat + mouse) TSP-1, 5'-GGCCAAGATCTATCCAGCCC-3' and 5'-GCCCACACAGCGTCCAGTA-3'; P450 2B11, 5'-AAATCCTTCCTCAGGCTCCAA-3' and 5'-GCCTCCCGTATGGCGTCTAT-3'. qPCR mixtures containing 8 μl of SYBR Green PCR Master Mix, 4 μl of cDNA, 1 μl of forward or reverse primer and 2 μl of ddH_2O were loaded into triplicate wells of a 384-well plate (5 μl/well) and run through 40 cycles on ABS 7900HT sequence detection system (Applied Biosystems). C_t values determined for each gene were normalized to the 18S rRNA content of the same RNA sample. Data were expressed as relative RNA levels, mean ± SE for four individual tumors. The contribution of mouse (host) and rat (9L tumor-derived) TSP-1 RNA to total TSP-1 RNA in solid 9L tumors was determined as follows. 9L rat gliosarcoma tumors grown *s.c.* do not metastasize, and consequently, host (mouse) TSP-1 accounts for all the TSP-1 RNA detected in mouse liver. By measuring mouse liver TSP-1 RNA levels using both mouse-specific and total (mouse + rat) TSP-1 primer sets, both sets of TSP-1 primer pairs were shown to have similar intrinsic amplification efficiencies (ΔC_t = 12.0 and 12.7, respectively, when normalized relative to 18S rRNA). These two primer sets were used to assay 9L tumor RNA, where the total TSP-1 primer pair detected a substantially higher level of TSP-1 RNA than the mouse-specific TSP-1 primer pair, with rat TSP-1 corresponding to ~ 95% of the total TSP-1 RNA in untreated 9L tumors after factoring in the < 2-fold difference in intrinsic amplification efficiency noted above.

Preparation of Tumor Microsomes and Western Blotting

Frozen tumor samples were homogenized on ice in microsome preparation buffer (100 mM KPi, pH 7.5, 1 mM EDTA, 0.1 mM dithiothreitol, 0.1 mM phenylmethylsulfonyl fluoride), centrifuged at 12,000 g for 20 min at 4°C and the supernatant was collected. The pellet was resuspended in microsome preparation buffer and centrifuged again. The combined supernatants were centrifuged at 185,000 g for 60 min at 4°C. The pellets were washed and resuspended in microsome storage buffer (100 mM KPi, pH 7.5, 1 mM EDTA, 0.1 mM dithiothreitol, 0.1 mM phenylmethylsulfonyl fluoride, 20% glycerol). Protein concentrations were determined by Bio-Rad D_c Protein Assay kit. For Western blot analysis, microsomal protein (20 μg) was electrophoresed on 7.5% SDS-polyacrylamide gels and transferred to nitrocellulose membranes. Membranes were blocked with 3% fat-free milk in TBST (1 mM Tris-HCl pH 7.6, 150 mM sodium chloride, 0.1% Tween-20) and probed for 1 hr at room temperature with rabbit polyclonal anti-P450 2B11 antibody (1:2000 in blocking solution). The blot was washed and incubated with HRP-conjugated anti-rabbit IgG (1:3000 dilution). P450 2B11 protein was visualized with enhanced chemiluminescence detection reagent and exposed to Kodak X-OMAT blue film XB-1. A duplicate gel was stained with coomassie blue R-250 to confirm equal protein loading for each sample.

Statistical Analysis

Results were expressed as mean ± SE. Statistical significance of differences was assessed by two-tailed Student's *t* test or one-way ANOVA, implemented using Prism software (Version 4, GraphPad, San Diego, CA). $p < 0.05$ was considered statistically significant.

RESULTS

Impact of intratumoral P450 on anti-angiogenic action of metronomic CPA

Metronomic CPA treatment substantially regresses 9L tumors, whereas CPA treatment on an MTD schedule leads to only a modest delay in tumor growth (13). In the case of 9L tumors that express P450 2B11, a highly efficient catalyst of CPA activation, the regression induced by metronomic CPA is more rapid and substantially more complete (20). To better understand the mechanism underlying this enhanced anti-tumor response, we investigated the impact of metronomic CPA on tumor vascularization, both in 9L tumors and in 9L tumors expressing P450 2B11 (9L/2B11 tumors). Untreated 9L tumors were highly vascularized, as visualized by CD31 immunostaining (Fig. 1A). The first cycle of metronomic CPA treatment had no effect on tumor microvessel density, while the second CPA treatment induced a notable decrease in microvessel density in both 9L tumors and 9L/2B11 tumors (Fig. 1B). 9L tumor microvessel density continued to decrease slowly after the third CPA injection, with no microvessel size selection apparent based on the sizes of the remaining blood vessels. In addition, double immunostaining for CD31 and smooth muscle actin-α revealed a transient increase in the pericyte coverage of tumor blood vessels 3 days after the second CPA treatment (Fig. S1; day 9, $p<0.01$), which returned to the basal, untreated level by day 12 and remained at that level through the fourth CPA injection.

To confirm these findings using an independent approach, a single cell suspension was prepared from freshly excised tumor tissue, and endothelial cells were labeled with anti-CD31 antibody and quantified as a percentage of the total tumor cell population by flow cytometry. In untreated tumors, 2.79 ± 0.56% (9L) or 2.13 ± 0.59% (9L/2B11) of the cells were CD31-positive (Fig. 1C). Following the first CPA treatment cycle, after a small change on day 1, the percentage of endothelial cells decreased to 2.11 ± 0.19% (9L) or 1.75 ± 0.42% (9L/2B11) on day 3 and partially recovered to near pretreatment levels by day 6. A more substantial reduction in the endothelial cell population was observed 3 days after the second CPA injection (Fig. 1C; day 9 vs. day 6, $p<0.01$) and the recovery by day 12 was more limited. This finding is consistent

with observations in Lewis lung cancer xenografts, where endothelial cell apoptosis was maximal by days 1–3 after the second cycle of CPA treatment (12). A similar endothelial cell response pattern was observed for 9L/2B6 tumors (Fig. 1C; also see Fig. 1A, bottom), which express the CPA-activating P450 2B6 and are also chemosensitized to CPA, albeit less effectively than in the case of P450 2B11. The successive decreases in endothelial cells relative to the overall tumor cell population seen with each round of CPA treatment indicate that the damage to the tumor vasculature cannot be fully repaired prior to the next CPA treatment cycle. As such, the damage accumulates, and by day 6 after the fourth CPA treatment endothelial cells account for only 0.34–0.44% of the total tumor cell population, corresponding to an 85% reduction from the initial level. The same response was seen in all three tumor types (9L, 9L/2B11, 9L/2B6), indicating that intratumoral expression of a CPA-activating P450 enzyme has little impact on the anti-angiogenic activity of metronomic CPA.

To better understand the role of anti-angiogenesis in metronomic CPA-induced tumor regression, we compared the changes in tumor size to the changes in vascular density during the course of CPA treatment for both 9L and 9L/2B11 tumors (Fig. 1B). Overall tumor cell density was also examined by hematoxylin-eosin staining (Fig. 2). The first CPA treatment cycle had no discernable effect on tumor growth. As the tumor volume continued to expand, the initial decrease in endothelial cell population seen at day 3 (Fig. 1C) was reversed by day 6, at which time tumor microvessel density and overall tumor cell density were unchanged. Although 9L and 9L/2B11 tumors both continued to grow in volume for the first three days after the second CPA injection (Fig. 1B), tumor cell density (Fig. 2) and vascularization (Fig. 1C) both decreased substantially during this time period. Tumor regression after the third and fourth CPA injections was accompanied by continued decreases in the endothelial cell population and microvessel density. Thus, the second CPA cycle triggers serious and irreversible damage to the tumor vasculature, which could be an important factor in the subsequent decrease in tumor cell density. In addition, the anti-angiogenic responses to metronomic CPA precede the onset of tumor regression for both 9L and 9L/2B11 tumors, which supports the hypothesis that anti-angiogenesis contributes to the observed anti-tumor activity.

Impact of metronomic CPA on angiogenesis inhibitor TSP-1

TSP-1, an endogenous angiogenesis inhibitor, may be expressed in 9L tumor cells, which are of rat origin, and in tumor-associated host stromal cells, including endothelial cells, pericytes and fibroblasts, which are of mouse origin. Species-specific qPCR primers were therefore designed to specifically monitor the expression of tumor cell (rat) and host (mouse) TSP-1 RNA, as well as total (rat + mouse) TSP-1 RNA. Similarly, antibodies to mouse TSP-1 (antibody sc-12312) or to rat + mouse TSP-1 (antibody MS-421) were used to monitor TSP-1 protein.

In untreated 9L tumors, ~95% of total TSP-1 RNA is 9L cell-derived (rat TSP-1), with the other 5% derived from host stromal cells, as determined by qPCR analysis using liver TSP-1 RNA as a reference control (see Materials and Methods). Total (rat + mouse) tumor-associated TSP-1 RNA varied up to ~ 2-fold following metronomic CPA treatment (Fig. 3C; one-way ANOVA, $p = 0.36$). This reflects the composite profile of 9L cell TSP-1 RNA, which progressively declined in response to metronomic CPA (Fig. 3A), and host cell TSP-1 RNA, which increased transiently after the first two CPA injections (Fig. 3B). Immunohistochemical staining of tumor sections with anti-total TSP-1 antibody MS-421 (Fig. 3D) revealed a decline after two cycles of CPA treatment, in agreement with the decrease in 9L tumor cell TSP-1 RNA. CD31/TSP-1 double immunostaining using host TSP-1-specific antibody revealed a small number of blood vessels with TSP-1 protein in perivascular cells (Fig. 3E), but not in

the associated endothelial cells. Thus, tumor cell and host cell TSP-1 respond differently to metronomic CPA, suggesting that each plays a distinct role in the overall anti-angiogenic effect.

Intratumoral P450 2B11 expression augments 9L tumor apoptosis

Next, we investigated why metronomic CPA-treated 9L/2B11 tumors regress earlier and more completely than 9L control tumors, given the similar anti-angiogenic responses of both tumors. To test whether this difference reflects enhanced killing of the 9L tumor cells by intracellular, P450-dependent activation of CPA to 4-OH-CPA, tumor cryosections were labeled by TUNEL assay (Fig. 4A) and the apoptotic index was determined for 9L and 9L/2B11 tumors (Fig. 4B). Very few apoptotic cells were detected in untreated tumors. One day after the first CPA injection, although there were only small changes in the tumor-associated endothelial cell population (Fig. 1C), the apoptotic index increased significantly in both 9L and 9L/2B11 tumors, indicating a direct anti-tumor cytotoxic effect of 4-OH-CPA. In 9L/2B11, but not 9L tumors, the increase in apoptosis was sustained for three days, whereas by day 6, the apoptotic index returned to near basal, pretreatment level in both 9L tumor types (Fig. 4B). During the second cycle of CPA treatment, 9L tumors only showed a small, transient increase, whereas in 9L/2B11 tumors, apoptosis increased significantly through the third day, highlighting the P450 2B11-dependent enhancement of tumor cell killing. The enhanced tumor cell cytotoxic response conferred by P450 2B11 is thus distinct from the anti-angiogenic action of metronomic CPA, which does not differ between 9L and 9L/2B11 tumors.

Response of P450 2B11 protein to metronomic CPA

The impact of CPA treatment on P450 2B11 RNA and protein was investigated to better understand how intratumoral expression of P450 2B11 contributes to the anti-tumor effect of metronomic CPA. P450 2B11 RNA levels were unchanged in the first two cycles of CPA treatment, as determined by qPCR (Fig. 5A). Western blot analysis of microsomal proteins extracted from 9L/2B11 tumors indicated no change in 2B11 protein after the first CPA injection. However, by day 12, i.e., 6 days after the second CPA injection, 2B11 protein levels were substantially decreased in all 9L/2B11 tumors (Fig. 5B). Immunohistochemical staining revealed that 29–68% of the cells were 2B11-positive in individual untreated 9L/2B11 tumors (average = 55%; n = 4 tumors), as compared to 90–95% 2B11-positive cells in the original retrovirus-infected cell population used to implant the 9L/2B11 tumors (Fig. 6A and data not shown). The number of P450 2B11-positive cells was unchanged after the first CPA injection, but decreased after the second CPA treatment (Fig. 6A), consistent with the Western blot results. Similar changes were seen in 9L/2B6 tumors, where repopulation of the residual tumor mass with P450-deficient cells was apparent by day 24 (Fig. 6A, bottom). Many of the remaining P450-positive cells became enlarged and multinucleated in response to metronomic CPA, both in the case of 9L/2B11 and 9L/2B6 tumors (Fig. 6B).

DISCUSSION

When cancer chemotherapeutic drugs are administered on a traditional MTD schedule, an obligatory rest period between treatment cycles allows for the recovery of sensitive host tissues (e.g., bone marrow) but also provides an opportunity for recovery and regrowth of tumor cells and tumor-associated endothelial cells. This problem can be circumvented by administration of CPA using a regular, repeating (metronomic) schedule, which is associated with anti-angiogenic activity (12) and has received much attention as a possible alternative to traditional MTD regimens. When metronomic CPA is combined with P450 gene-directed enzyme-prodrug therapy, tumor cell expression of a CPA-activating P450 enzyme further enhances activity and leads to a sustained anti-tumor response (13). Presently, we investigate the impact of intratumoral P450-catalyzed CPA activation on tumor-associated endothelial cells and the role of liver vs. tumor cell P450 metabolism in the enhanced anti-tumor response. Our findings

lead us to conclude that a close collaboration between hepatic P450 prodrug activation and intratumoral prodrug activation catalyzed by the P450 transgene is required to maximize the therapeutic response in this gene therapy model. Thus, while liver P450 prodrug activation alone is sufficient to induce the anti-angiogenic effect that is a hallmark of metronomic CPA, the small tumors that result retain strong proliferative potential and often become angiogenesis-independent. Moreover, the anti-angiogenic action of metronomic CPA suppresses the uptake of liver-derived 4-OH-CPA *(J Ma & DJ Waxman, unpublished data)*, thereby rendering the tumor cells resistant to direct cytotoxicity. However, when metronomic CPA is combined with intratumoral expression of a CPA-activating P450 enzyme, the anti-angiogenic effect of liver-activated CPA ('killing from the outside') collaborates with intratumoral P450-dependent cytotoxicity ('killing from the inside') to enhance overall tumor cell killing, substantially prolonging the tumor-free period after cessation of drug treatment.

An unanticipated finding of the present study was the absence of an effect of intratumoral P450 expression on the anti-angiogenic action of metronomic CPA. Although this finding could be viewed as supporting the hypothesis that the direct anti-tumor actions of metronomic CPA, rather than its anti-angiogenic effects, are responsible for the anti-tumor response seen in the context of P450 GDEPT, that interpretation is not consistent with our earlier finding that regression of 9L/P450 tumors is induced by a metronomic, anti-angiogenic CPA schedule but not by MTD CPA treatment (13). Moreover, various drug-resistant tumor models used in earlier studies confirm the critical role of anti-angiogenesis in the anti-tumor activity of metronomic CPA (12). An important feature of P450-based GDEPT using CPA is that the active metabolite, 4-OH-CPA, readily diffuses across cell membranes and shows a strong bystander cytotoxic effect on surrounding P450-deficient tumor cells, both *in vitro* (22) and *in vivo* (7). However, this bystander cytotoxicity does not extend to include tumor-associated endothelial cells (Fig. 1). This discrepancy could relate to the location of endothelial cells within the tumor. The anatomical structure of the liver determines that hepatocytes have direct access to CPA in the blood, enabling liver P450 to dominate CPA metabolism following *i.p.* drug administration. The activated metabolite, 4-OH-CPA, enters systemic circulation and reaches the tumor vasculature, where tumor-associated endothelial cells are the first cells exposed to 4-OH-CPA and its DNA cross-linking, cytotoxic decomposition product phosphoramide mustard. In contrast, 9L tumor cells have more limited access to circulating 4-OH-CPA (23), presumably reflecting the dysfunctional tumor vasculature. Moreover, in the case of 9L/2B11 tumors, 4-OH-CPA formed intratumorally needs to cross through both tumor stroma and endothelial basal membranes before it can reach tumor-associated endothelial cells. Thus, the extensive exposure of these endothelial cells to liver-derived 4-OH-CPA, coupled with their restricted access to 4-OH-CPA formed intratumorally, effectively limits the bystander killing of tumor-associated endothelial cells by tumor cell P450-derived 4-OH-CPA.

In addition to its anti-angiogenic activity, metronomic CPA shows direct cytotoxicity toward 9L tumor cells, particularly in tumors that express the canine P450 enzyme 2B11, which catalyzes CPA activation (4-hydroxylation) with high efficiency due to an atypically low K_m of ~70 μM (20,21). In 9L tumors, apoptosis induced by the first CPA treatment cycle was transient, while in 9L/2B11 tumors, tumor cell apoptosis increased substantially until day 3. Moreover, only a limited increase in 9L tumor cell apoptosis was observed following the second CPA treatment cycle, suggesting that those tumor cells that are in close proximity to the tumor vasculature and thus are readily accessible to liver-derived 4-OH-CPA were already removed in the first CPA cycle. Direct killing of the surviving tumor cells may thus occur less frequently in the subsequent cycles of CPA treatment. In the case of 9L/2B11 tumors, however, localized prodrug activation was associated with a significant increase in tumor cell apoptosis after the second CPA treatment. Three days after the second CPA injection, when tumor microvessel density and endothelial cell counts both dropped significantly, anti-angiogenesis likely begins to play an important role in the overall anti-tumor effect. An alternative way to induce strong

tumor cell cytotoxicity while retaining the anti-angiogenic activity of CPA is to combine metronomic treatment with a traditional MTD or bolus schedule (24,25).

Once activated by P450 enzymes, CPA metabolites generated intratumorally kill P450 2B11-positive tumor cells as well as bystander tumor cells. The bystander killing of P450-negative tumor cells is supported by the fact that more complete overall tumor regression is achieved in 9L/2B11 tumors than 9L tumors (20), despite the fact that only 29–68% of the tumor cells express P450 2B11 at the time of the initial CPA treatment (Fig. 6). Tumor cell P450 2B11 protein, but not RNA, was substantially decreased beginning with the second CPA treatment cycle, whereas in the case of another P450 tumor model, 9L/2B6, P450 protein and RNA levels were both unchanged after two CPA cycles (unpublished data). This difference may reflect the 20-fold lower K_m (CPA) and 28-fold higher V_{max}/K_m ratio exhibited by P450 2B11 compared to P450 2B6 (20), which can result in high intracellular levels of acrolein or other P450 protein-binding metabolites derived from 4-OH-CPA (26,27) and, consequently, P450 protein degradation. The gradual loss of intratumoral P450 protein following metronomic CPA treatment indicates that repeated delivery of the therapeutic P450 gene will likely be required to optimize P450-based GDEPT treatment strategies. The death of P450-expressing 4-OH-CPA-producing ‘factory’ tumor cells can be delayed, however, by introduction of anti-apoptotic factors, which increase the net production of cytotoxic drug metabolites without conferring drug resistance (22,28).

The decline of P450-expressing tumor cells during the course of metronomic CPA treatment was accompanied by a significant enlargement of many of the remaining P450-positive cells, both in the case of 9L/2B11 tumors and 9L/2B6 tumors. Alkylating reagents such as CPA induce DNA crosslinks which eventually leads to programmed cell death (29). Cell cycle check-points are often perturbed in tumor cells, which can lead to delayed apoptosis and the induction of mitotic catastrophe, as observed in some cytotoxin-treated tumors (30,31). The enlarged 9L/P450 cells seen in the metronomic CPA-treated tumors may thus reflect CPA-induced DNA damage culminating in mitotic catastrophe. It is unclear whether the P450 protein that accumulates in these enlarged cells retains CPA metabolic activity.

The endogenous angiogenesis inhibitor TSP-1 is expressed in both host tissues (32) and tumor cells (33–36). Its deficiency leads to increased tumor growth and enhanced tumor angiogenesis (37). The anti-angiogenic activity of TSP-1 involves multiple mechanisms, including suppression of endothelial cell migration, induction of apoptosis with increased expression of Fas ligand in proliferating endothelial cells (37,38), inhibition of VEGF mobilization in the extracellular matrix, and reduction of blood flow by blocking nitric oxide/cGMP-induced relaxation of vascular smooth muscle cells (39,40). The function of 9L cell-derived TSP-1, presently shown to comprise ~95% of the tumor-associated TSP-1 RNA in untreated tumors, is unclear, but it may inhibit the growth of tumor metastases as suggested for other tumors (41–43). Metronomic CPA was presently shown to decrease tumor cell (rat) TSP-1 expression while increasing host (mouse) TSP-1 such that a substantial fraction of the 9L tumor-associated TSP-1 is of mouse origin after two CPA treatment cycles. CD31/TSP-1 double staining revealed the expression of TSP-1 in host-derived perivascular cells, which is likely an important source of the host TSP-1 detected by qPCR. Metronomic CPA induction of TSP-1 has been also observed in perivascular cells associated with Lewis lung cancer and B16F10 melanoma tumors, where either host cell- or tumor cell-derived TSP-1 may augment the anti-tumor effect of metronomic CPA (35). Although the number of TSP-1-positive blood vessels is low in 9L tumors (2–8 vessels/section), the close spatial association between perivascular cells and endothelial cells may facilitate interactions between TSP-1 and its endothelial cell membrane receptor, CD36.

In conclusion, while anti-angiogenesis clearly contributes to the overall anti-tumor effect of metronomic CPA, the anti-angiogenic response is very similar for 9L and 9L/2B11 tumors. It is also apparent, however, that the tumor cell population has poor access to liver-derived 4-OH-CPA, especially in the later cycles of metronomic CPA treatment, hence the requirement of intratumoral P450 gene delivery and intratumoral prodrug activation for tumor cell elimination leading to a sustained anti-tumor response. Further increases in intratumoral CPA activation could potentially be achieved by direct intratumoral delivery of CPA (23) or by inhibition or down-regulation of liver P450 or P450 reductase (44–46), both of which would be expected to increase CPA access to tumor-expressed P450 enzymes and enhance intratumoral prodrug activation. Whether the resultant increase in tumor cell-derived 4-OH-CPA at the expense of liver-derived 4-OH-CPA is consistent with maintenance of the overall anti-tumor effect, requires further investigation.

Supplementary Material

Refer to Web version on PubMed Central for supplementary material.

ABBREVIATIONS

CPA, cyclophosphamide; FACS, fluorescence-activated cell sorter; GDEPT, gene-directed enzyme prodrug therapy; MTD, maximum tolerated dose; qPCR, quantitative real-time PCR; TSP-1, thrombospondin-1.

ACKNOWLEDGEMENTS

We thank Dr. Youssef Jounaidi for providing the 9L/2B11 and 9L/2B6 cells used in this study, and Chong-Sheng Cheng for assistance in flow cytometry sample preparation.

This study was supported in part by NIH grant CA49248 (to D.J.W.).

REFERENCES

1. Foehr ED, Lorente G, Kuo J, Ram R, Nikolich K, Urfer R. Targeting of the receptor protein tyrosine phosphatase beta with a monoclonal antibody delays tumor growth in a glioblastoma model. Cancer Res 2006;66:2271–2278. [PubMed: 16489031]
2. Chu TC, Marks JW 3rd, Lavery LA, et al. Aptamer:toxin conjugates that specifically target prostate tumor cells. Cancer Res 2006;66:5989–5992. [PubMed: 16778167]
3. Kirpotin DB, Drummond DC, Shao Y, et al. Antibody targeting of long-circulating lipidic nanoparticles does not increase tumor localization but does increase internalization in animal models. Cancer Res 2006;66:6732–6740. [PubMed: 16818648]
4. Jounaidi Y, Hecht JE, Waxman DJ. Retroviral transfer of human cytochrome P450 genes for oxazaphosphorine-based cancer gene therapy. Cancer Res 1998;58:4391–4401. [PubMed: 9766669]
5. Tyminski E, Leroy S, Terada K, et al. Brain tumor oncolysis with replication-conditional herpes simplex virus type 1 expressing the prodrug-activating genes, CYP2B1 and secreted human intestinal carboxylesterase, in combination with cyclophosphamide and irinotecan. Cancer Res 2005;65:6850–6857. [PubMed: 16061668]
6. Jounaidi Y, Waxman DJ. Use of replication-conditional adenovirus as a helper system to enhance delivery of P450 prodrug-activation genes for cancer therapy. Cancer Res 2004;64:292–303. [PubMed: 14729637]
7. Samel S, Keese M, Lux A, et al. Peritoneal cancer treatment with CYP2B1 transfected, microencapsulated cells and ifosfamide. Cancer gene therapy 2006;13:65–73. [PubMed: 16096652]
8. Salmons B, Lohr M, Gunzburg WH. Treatment of inoperable pancreatic carcinoma using a cell-based local chemotherapy: results of a phase I/II clinical trial. J Gastroenterol 2003;38:78–84. [PubMed: 12698877]

9. Braybrooke JP, Slade A, Deplanque G, et al. Phase I study of MetXia-P450 gene therapy and oral cyclophosphamide for patients with advanced breast cancer or melanoma. Clin Cancer Res 2005;11:1512–1520. [PubMed: 15746054]
10. Folkman J. Tumor angiogenesis: therapeutic implications. N Engl J Med 1971;285:1182–1186. [PubMed: 4938153]
11. Jain RK, Duda DG, Clark JW, Loeffler JS. Lessons from phase III clinical trials on anti-VEGF therapy for cancer. Nat Clin Pract Oncol 2006;3:24–40. [PubMed: 16407877]
12. Browder T, Butterfield CE, Kraling BM, et al. Antiangiogenic scheduling of chemotherapy improves efficacy against experimental drug-resistant cancer. Cancer Res 2000;60:1878–1886. [PubMed: 10766175]
13. Jounaidi Y, Waxman DJ. Frequent, moderate-dose cyclophosphamide administration improves the efficacy of cytochrome P-450/cytochrome P-450 reductase-based cancer gene therapy. Cancer Res 2001;61:4437–4444. [PubMed: 11389073]
14. Man S, Bocci G, Francia G, et al. Antitumor effects in mice of low-dose (metronomic) cyclophosphamide administered continuously through the drinking water. Cancer Res 2002;62:2731–2735. [PubMed: 12019144]
15. Munoz R, Man S, Shaked Y, et al. Highly efficacious nontoxic preclinical treatment for advanced metastatic breast cancer using combination oral UFT-cyclophosphamide metronomic chemotherapy. Cancer Res 2006;66:3386–3391. [PubMed: 16585158]
16. Klement G, Baruchel S, Rak J, et al. Continuous low-dose therapy with vinblastine and VEGF receptor-2 antibody induces sustained tumor regression without overt toxicity. J Clin Invest 2000;105:R15–R24. [PubMed: 10772661]
17. Colleoni M, Orlando L, Sanna G, et al. Metronomic low-dose oral cyclophosphamide and methotrexate plus or minus thalidomide in metastatic breast cancer: antitumor activity and biological effects. Ann Oncol 2006;17:232–238. [PubMed: 16322118]
18. Young SD, Whissell M, Noble JC, Cano PO, Lopez PG, Germond CJ. Phase II Clinical Trial Results Involving Treatment with Low-Dose Daily Oral Cyclophosphamide, Weekly Vinblastine, and Rofecoxib in Patients with Advanced Solid Tumors. Clin Cancer Res 2006;12:3092–3098. [PubMed: 16707607]
19. Bocci G, Tuccori M, Emmenegger U, et al. Cyclophosphamide-methotrexate 'metronomic' chemotherapy for the palliative treatment of metastatic breast cancer. A comparative pharmacoeconomic evaluation. Ann Oncol 2005;16:1243–1252. [PubMed: 15905308]
20. Jounaidi Y, Chen C-S, Veal GJ, Waxman DJ. Enhanced antitumor activity of P450 prodrug-based gene therapy using the low Km cyclophosphamide 4-hydroxylase P450 2B11. Mol Cancer Ther 2006;5:541–555. [PubMed: 16546968]
21. Chen CS, Lin JT, Goss KA, He YA, Halpert JR, Waxman DJ. Activation of the anticancer prodrugs cyclophosphamide and ifosfamide: identification of cytochrome P450 2B enzymes and site-specific mutants with improved enzyme kinetics. Mol Pharmacol 2004;65:1278–1285. [PubMed: 15102956]
22. Schwartz PS, Chen CS, Waxman DJ. Enhanced bystander cytotoxicity of P450 gene-directed enzyme prodrug therapy by expression of the antiapoptotic factor p35. Cancer Res 2002;62:6928–6937. [PubMed: 12460909]
23. Chen CS, Jounaidi Y, Su T, Waxman DJ. Enhancement of intratumoral cyclophosphamide pharmacokinetics and anti-tumor activity in a P450 2B11-based cancer gene therapy model. Cancer gene therapy. 2007
24. Shaked Y, Emmenegger U, Francia G, et al. Low-dose metronomic combined with intermittent bolus-dose cyclophosphamide is an effective long-term chemotherapy treatment strategy. Cancer Res 2005;65:7045–7051. [PubMed: 16103050]
25. Pietras K, Hanahan D. A multitargeted, metronomic, and maximum-tolerated dose "chemoswitch" regimen is antiangiogenic, producing objective responses and survival benefit in a mouse model of cancer. J Clin Oncol 2005;23:939–952. [PubMed: 15557593]
26. Marinello AJ, Bansal SK, Paul B, et al. Metabolism and binding of cyclophosphamide and its metabolite acrolein to rat hepatic microsomal cytochrome P-450. Cancer Res 1984;44:4615–4621. [PubMed: 6380709]

27. Uchida K, Kanematsu M, Sakai K, et al. Protein-bound acrolein: Potential markers for oxidative stress. PNAS 1998;95:4882–4887. [PubMed: 9560197]

28. Waxman DJ, Schwartz PS. Harnessing apoptosis for improved anticancer gene therapy. Cancer Res 2003;63:8563–8572. [PubMed: 14695163]

29. Schwartz PS, Waxman DJ. Cyclophosphamide induces caspase 9-dependent apoptosis in 9L tumor cells. Mol Pharmacol 2001;60:1268–1279. [PubMed: 11723234]

30. Illidge TM, Cragg MS, Fringes B, Olive P, Erenpreisa JA. Polyploid giant cells provide a survival mechanism for p53 mutant cells after DNA damage. Cell biology international 2000;24:621–633. [PubMed: 10964452]

31. Castedo M, Perfettini JL, Roumier T, Andreau K, Medema R, Kroemer G. Cell death by mitotic catastrophe: a molecular definition. Oncogene 2004;23:2825–2837. [PubMed: 15077146]

32. Sezaki S, Hirohata S, Iwabu A, et al. Thrombospondin-1 is induced in rat myocardial infarction and its induction is accelerated by ischemia/reperfusion. Exp Biol Med (Maywood) 2005;230:621–630. [PubMed: 16179730]

33. Tringler B, Grimm C, Sliutz G, et al. Immunohistochemical expression of thrombospondin-1 in invasive vulvar squamous cell carcinoma. Gynecol Oncol 2005;99:80–83. [PubMed: 16009408]

34. Naumov GN, Bender E, Zurakowski D, et al. A model of human tumor dormancy: an angiogenic switch from the nonangiogenic phenotype. J Natl Cancer Inst 2006;98:316–325. [PubMed: 16507828]

35. Hamano Y, Sugimoto H, Soubasakos MA, et al. Thrombospondin-1 associated with tumor microenvironment contributes to low-dose cyclophosphamide-mediated endothelial cell apoptosis and tumor growth suppression. Cancer Res 2004;64:1570–1574. [PubMed: 14996710]

36. Moon Y, Bottone FG Jr. McEntee MF, Eling TE. Suppression of tumor cell invasion by cyclooxygenase inhibitors is mediated by thrombospondin-1 via the early growth response gene Egr-1. Mol Cancer Ther 2005;4:1551–1558. [PubMed: 16227405]

37. Sund M, Hamano Y, Sugimoto H, et al. Function of endogenous inhibitors of angiogenesis as endothelium-specific tumor suppressors. Proc Natl Acad Sci U S A 2005;102:2934–2939. [PubMed: 15710885]

38. Volpert OV, Zaichuk T, Zhou W, et al. Inducer-stimulated Fas targets activated endothelium for destruction by anti-angiogenic thrombospondin-1 and pigment epithelium-derived factor. Nat Med 2002;8:349–357. [PubMed: 11927940]

39. Isenberg JS, Ridnour LA, Perruccio EM, Espey MG, Wink DA, Roberts DD. Thrombospondin-1 inhibits endothelial cell responses to nitric oxide in a cGMP-dependent manner. Proc Natl Acad Sci U S A 2005;102:13141–13161. [PubMed: 16150726]

40. Isenberg JS, Hyodo F, Matsumoto K-I, et al. Thrombospondin-1 limits ischemic tissue survival by inhibiting nitric oxide-mediated vascular smooth muscle relaxation. Blood 2007;109:1945–1952. [PubMed: 17082319]

41. Rofstad EK, Graff BA. Thrombospondin-1-mediated metastasis suppression by the primary tumor in human melanoma xenografts. J Invest Dermatol 2001;117:1042–1049. [PubMed: 11710911]

42. Crawford SE, Flores-Stadler EM, Huang L, et al. Rapid growth of cutaneous metastases after surgical resection of thrombospondin-secreting small blue round cell tumor of childhood. Hum Pathol 1998;29:1039–1044. [PubMed: 9781638]

43. Volpert OV, Lawler J, Bouck NP. A human fibrosarcoma inhibits systemic angiogenesis and the growth of experimental metastases via thrombospondin-1. Proc Natl Acad Sci U S A 1998;95:6343–6348. [PubMed: 9600967]

44. Gu J, Chen CS, Wei Y, et al. A mouse model with liver-specific deletion and global suppression of the NADPH-cytochrome P450 reductase gene: characterization and utility for in vivo studies of cyclophosphamide disposition. The Journal of pharmacology and experimental therapeutics 2007;321:9–17. [PubMed: 17218484]

45. Huang Z, Raychowdhury MK, Waxman DJ. Impact of liver P450 reductase suppression on cyclophosphamide activation, pharmacokinetics and antitumoral activity in a cytochrome P450-based cancer gene therapy model. Cancer gene therapy 2000;7:1034–1042. [PubMed: 10917206]

46. Huang Z, Waxman DJ. Modulation of cyclophosphamide-based cytochrome P450 gene therapy using liver P450 inhibitors. Cancer gene therapy 2001;8:450–458. [PubMed: 11498765]

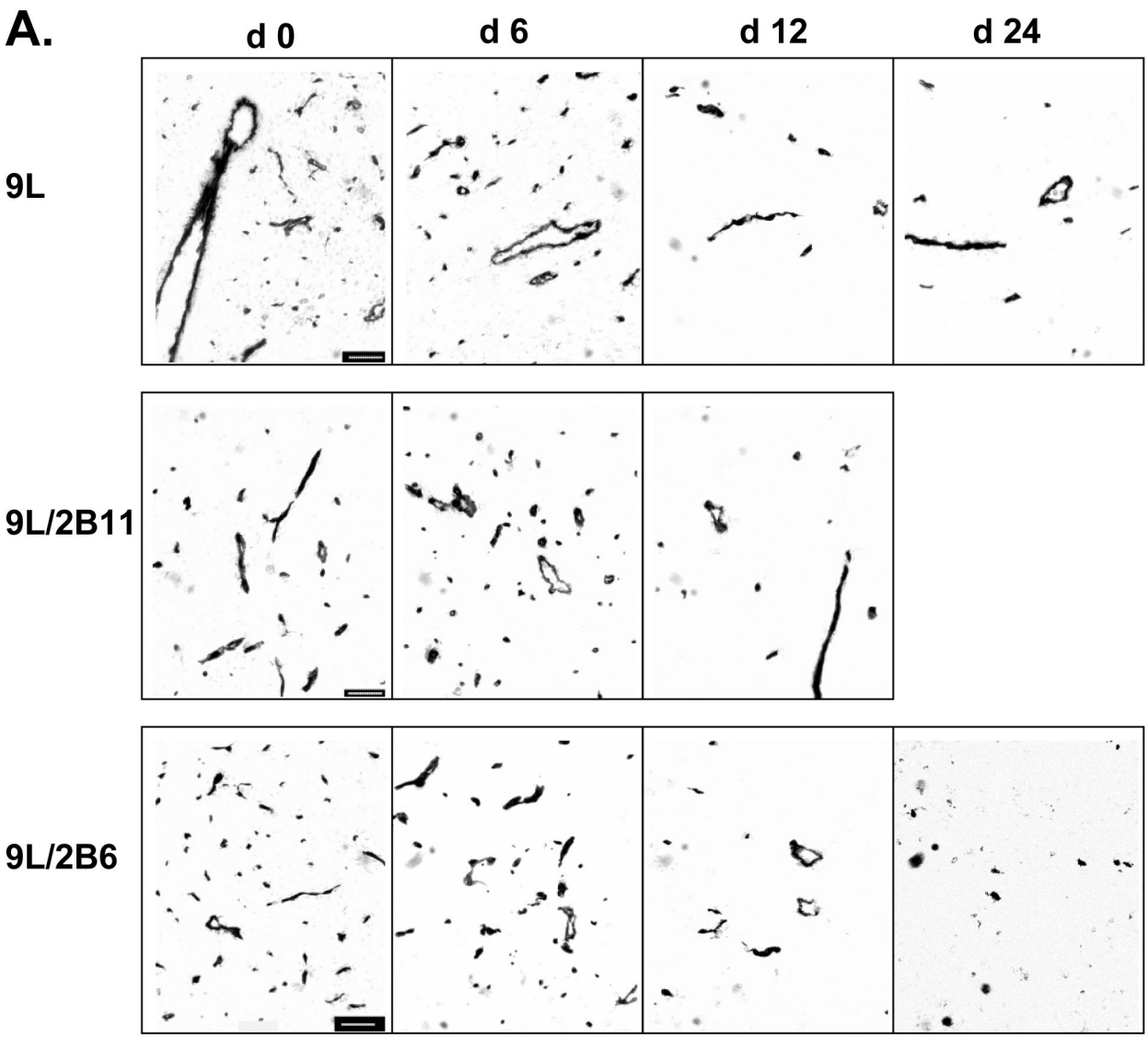

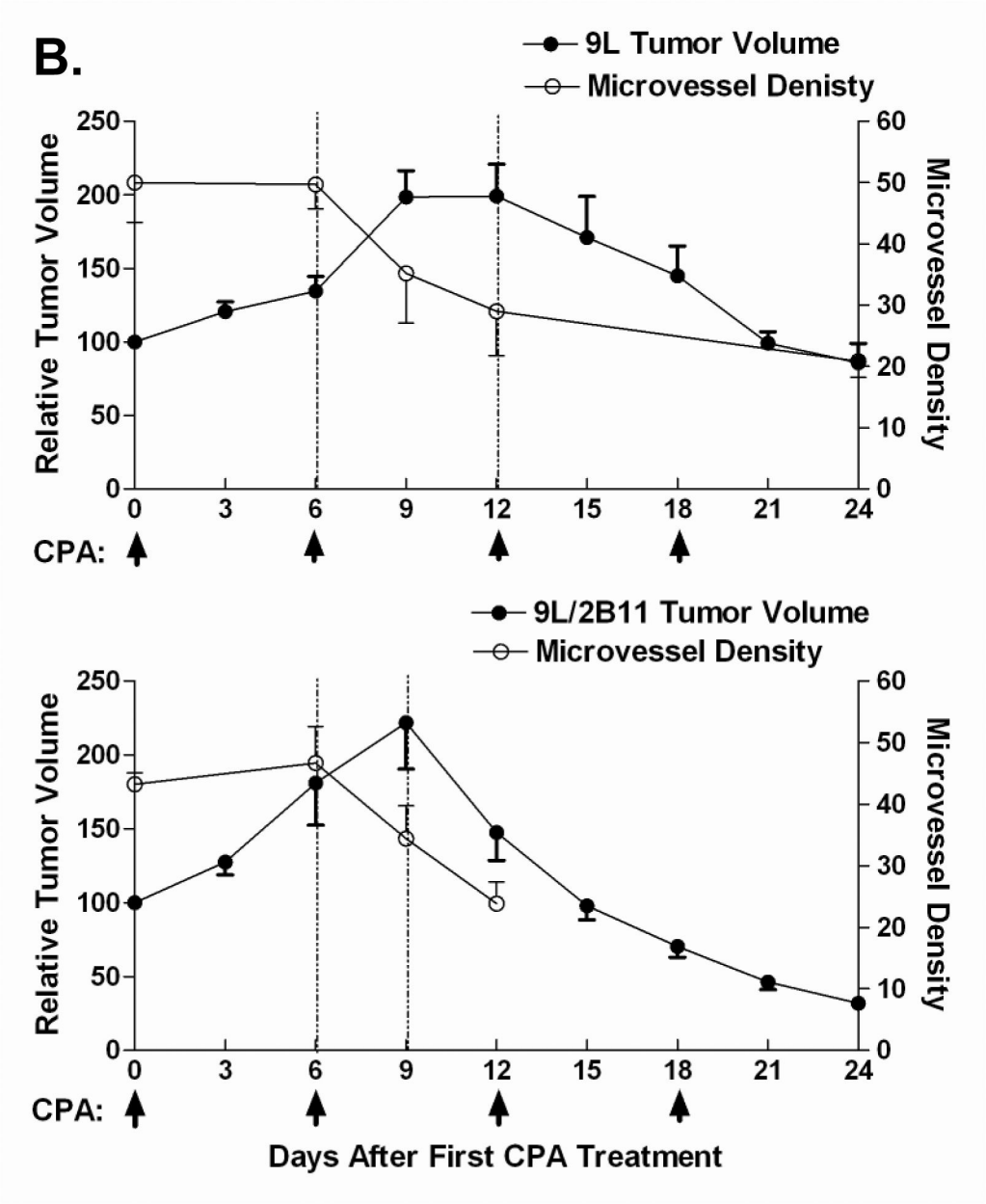

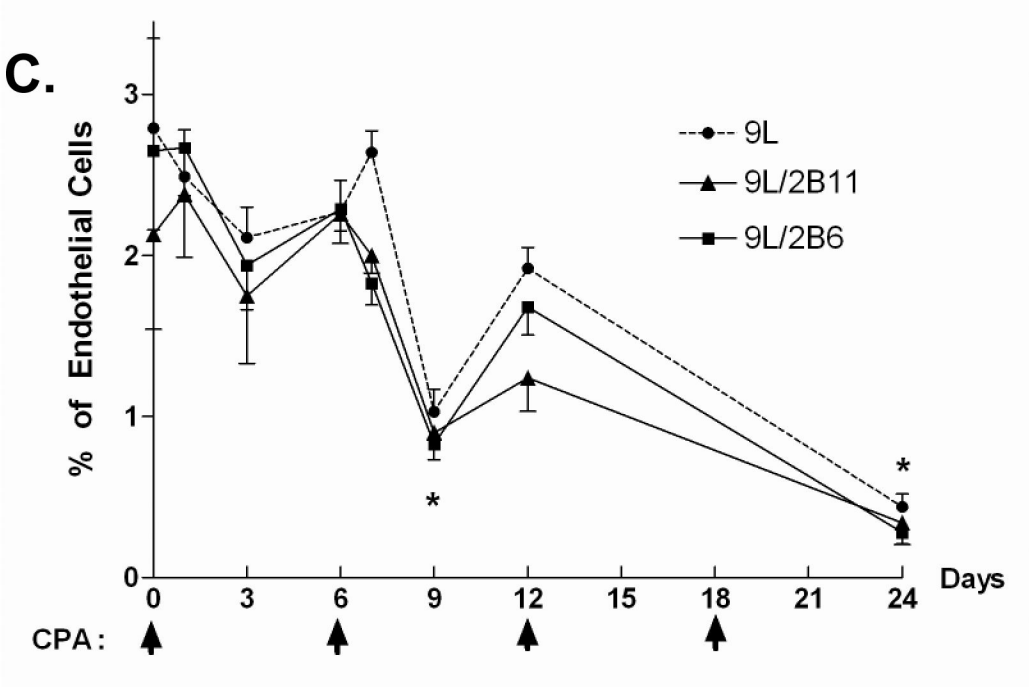

Figure 1. Impact of metronomic CPA treatment on growth, vascularity and endothelial cell population in 9L and 9L/2B tumors

A. *Scid* mice implanted *s.c.* with 9L control (top), 9L/2B11 (middle) or 9L/2B6 tumors (bottom) were treated with 140 mg CPA/kg body weight (*i.p.* injection) every 6 days beginning when the average tumor vol reached ~500 mm^3. Tumor blood vessels in 9L and 9L/P450 tumor sections were stained with antibody to the endothelial cell marker CD31 on days 0–24 after beginning of metronomic CPA treatment. Untreated 9L tumors were highly vascularized (day 0). Scale bar shown in the day 0 panels, 50 μm. **B.** 9L/2B11 tumors began to regress 3 days after the second CPA injection (lower panel) while 9L tumor regression began several days later (upper panel). A decrease in tumor microvessel density preceded the onset of tumor regression in both 9L and 9L/2B11 tumors, as delineated by the time window between the vertical dotted lines. Microvessel density is presented as the number of blood vessels per field at 400x magnification. **C.** Endothelial cells present in a single cell suspension prepared from freshly excised 9L, 9L/2B6 or 9L/2B11 tumors were labeled with FITC-conjugated CD31 antibody and quantified as a percentage of total tumor cell population by flow cytometry. Two cycles of metronomic CPA induced a 70% loss of tumor-associated endothelial cells, seen on day 9, which further decreased after the third and fourth CPA treatments (day 24). Asterisk indicates a significant difference in the percentage of endothelial cells compared to the most recent CPA treatment day (Student's *t*-test, $p < 0.05$). Arrows along the x-axis indicate days of CPA administration (panels B and C).

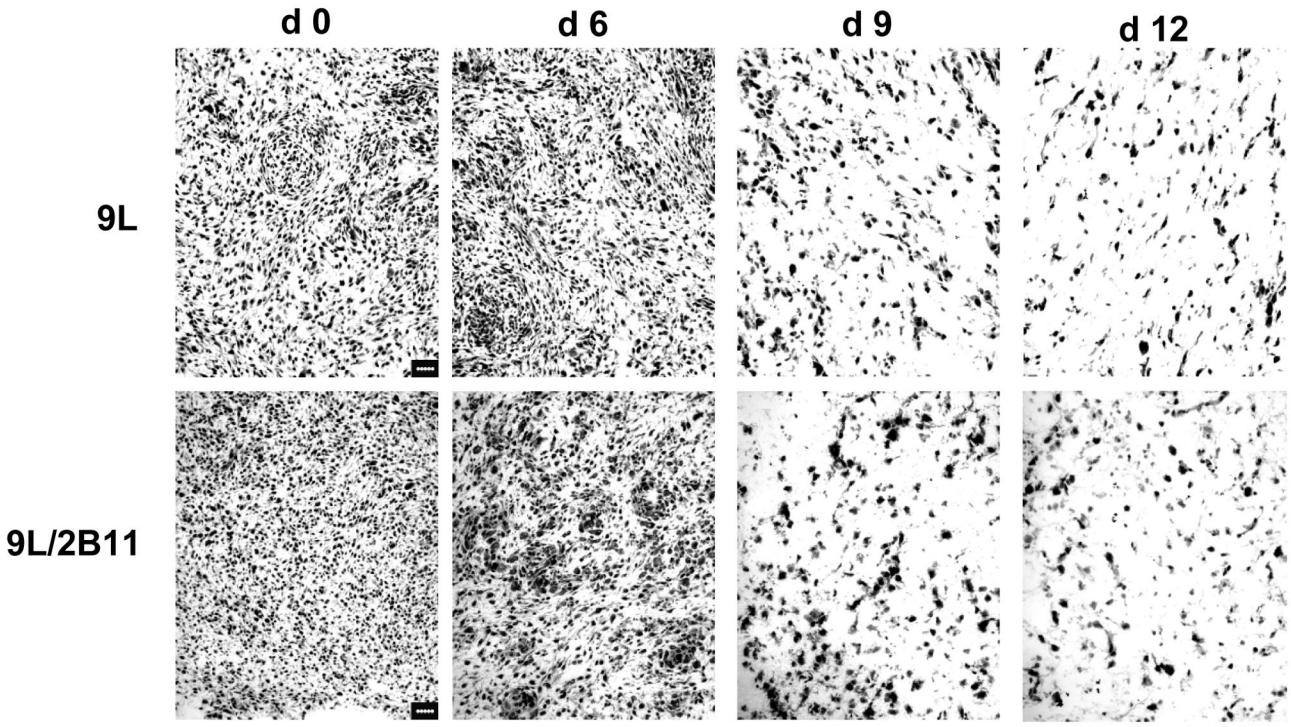

Figure 2. Reduced cell density in 9L and 9L/2B11 tumors treated by metronomic CPA

Hematoxylin-eosin staining revealed a decrease in tumor cell density on the 3rd and 6th days following the second CPA treatment (i.e., day 9 and day 12). Scale bar, 50 μm.

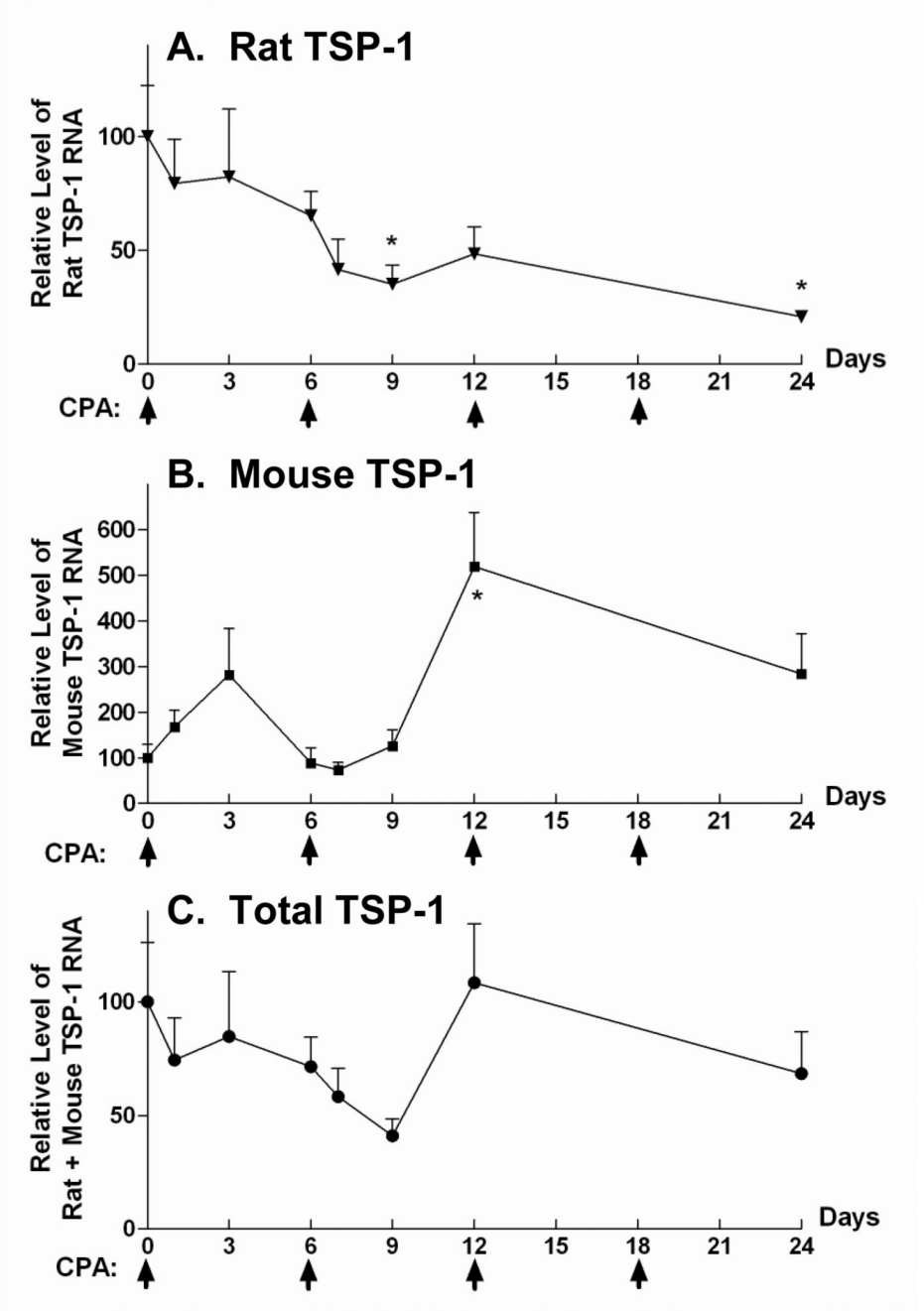

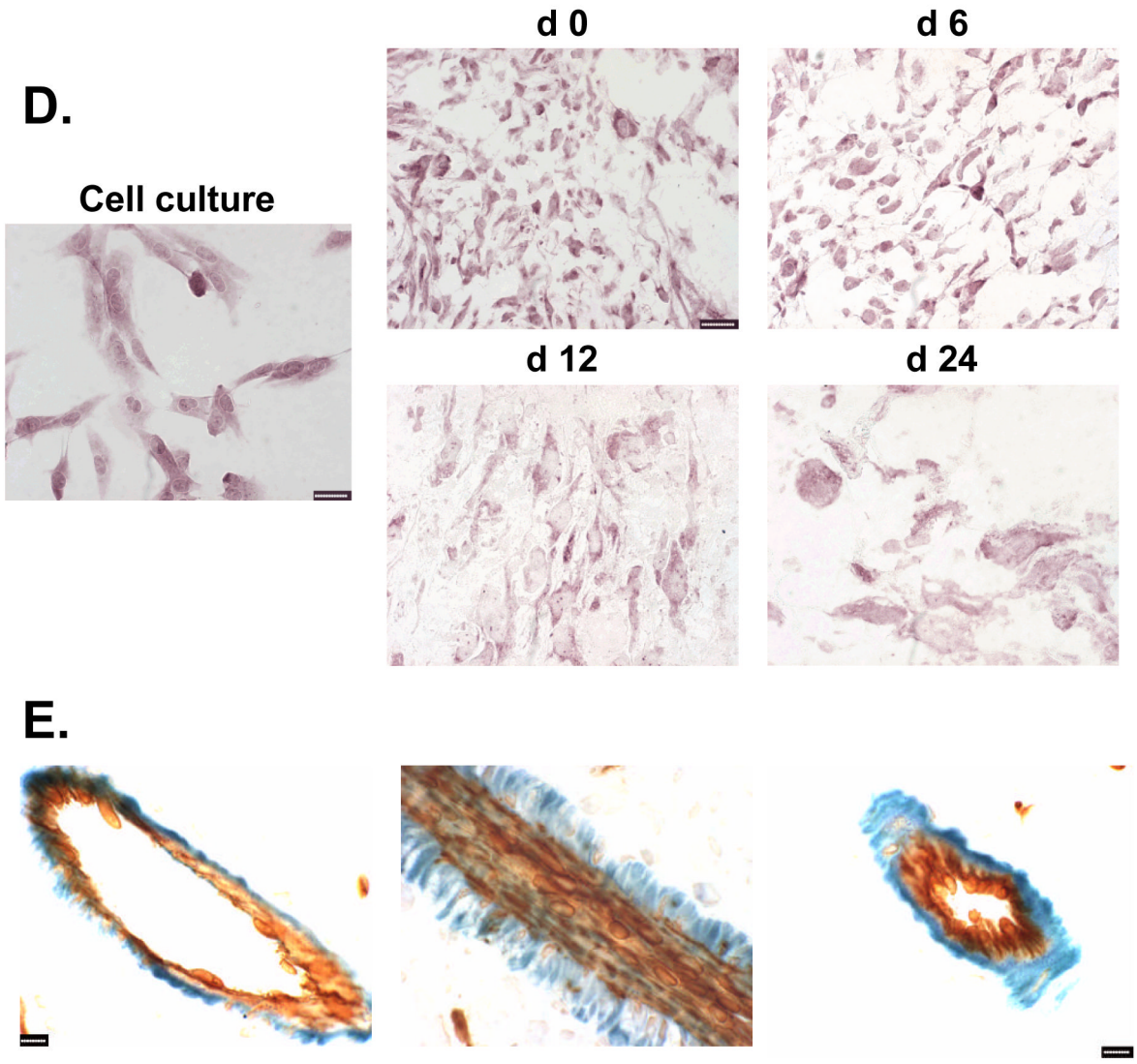

Figure 3. Differential expression of host or tumor cell-derived TSP-1 in metronomic CPA-treated 9L tumors

qPCR analysis of RNA encoding tumor cell-derived rat TSP-1 (**A**), host cell-produced mouse TSP-1 (**B**), and total (rat + mouse) TSP-1 (**C**). Asterisk indicates a significant change in TSP-1 RNA level when compared to day 0 (Student's *t*-test, $p < 0.05$). Arrows on X-axis indicate the days of CPA treatment. **D.** Antibody MS-421 was used to detect total (rat + mouse) TSP-1 protein in cultured 9L cells and in sections prepared from metronomic CPA-treated 9L tumors (day 0–24). Scale bar, 20 μm. **E.** CD31 (brown) and TSP-1 (blue, antibody sc-12312) double immunostaining revealed mouse TSP-1 staining of perivascular cells but not endothelial cells. Scale bar, 10 μm.

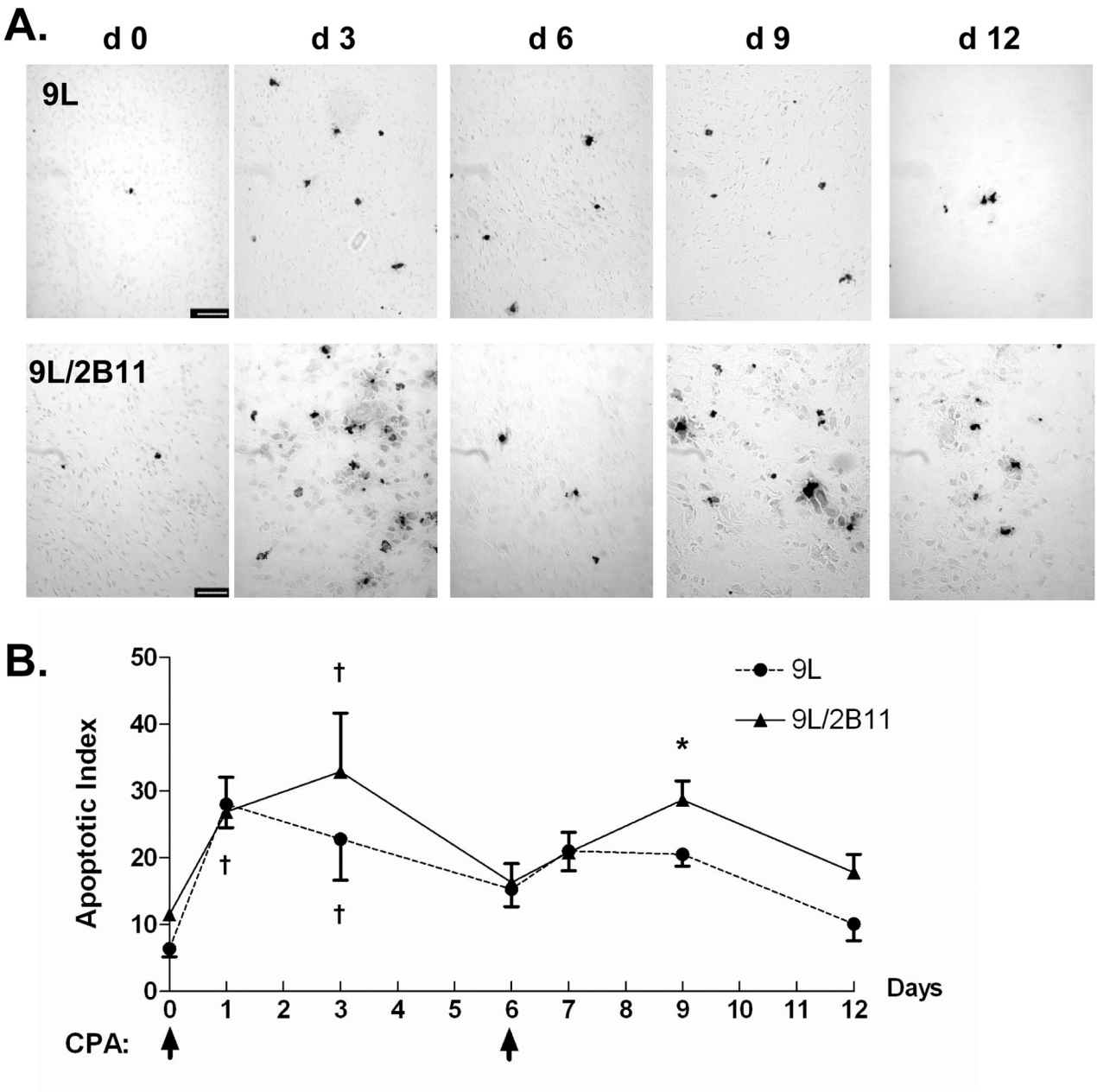

Figure 4. Impact of P450 on metronomic CPA-induced tumor cell apoptosis

A. Apoptotic cells in tumor cryosections prepared on day 0–12 following initiation of metronomic CPA treatment were labeled by TUNEL assay. Very few apoptotic cells were detected in untreated tumors. Scale bar, 50 μm. **B.** Quantification of TUNEL staining in the experiments represented in panel A, as described in Materials and Methods. Asterisk (*) indicates significantly different apoptosis levels between 9L and 9L/2B11 tumors (Student's *t*-test, $p < 0.05$). †, significant differences between day 0 vs. day 1 and day 3 (one-way ANOVA, $p < 0.05$).

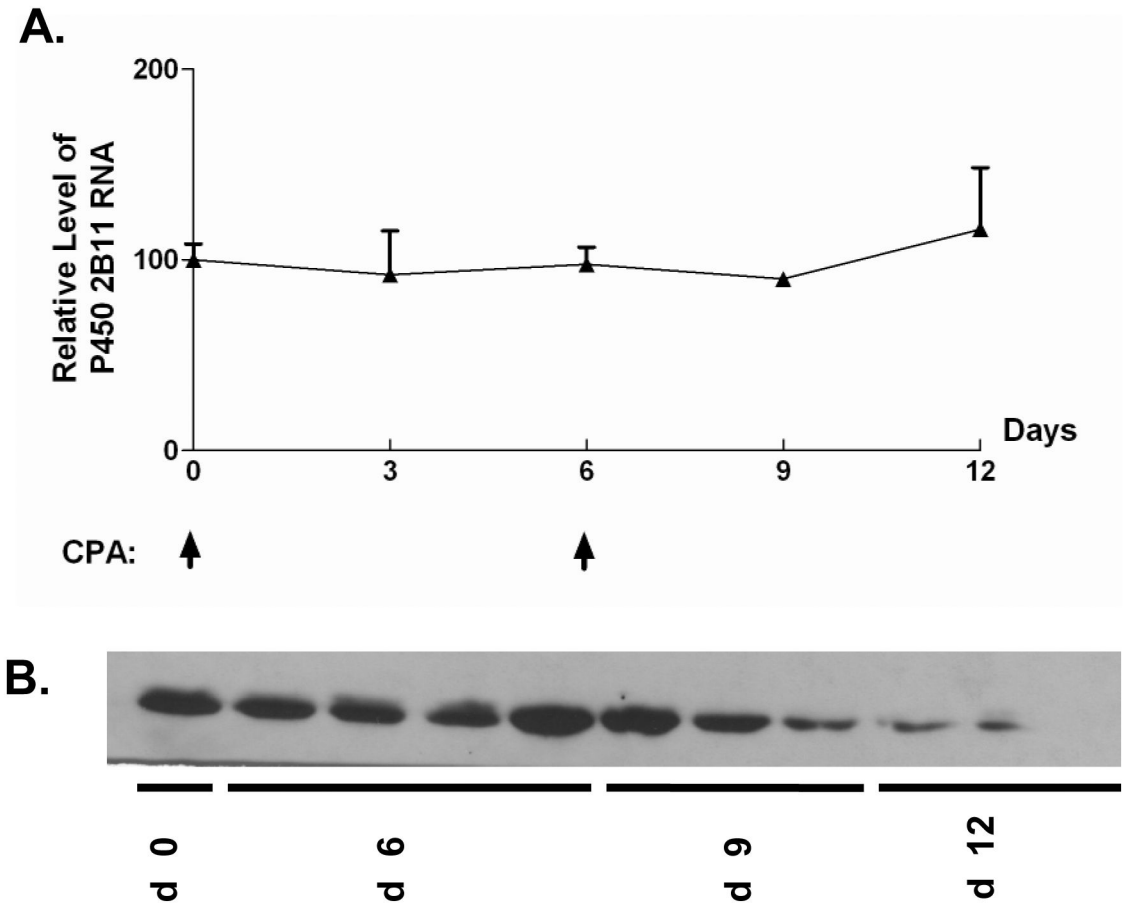

Figure 5. P450 2B11 RNA and protein levels during the course of metronomic CPA treatment

A. qPCR assay revealed that P450 2B11 RNA levels were unchanged in the first two cycles of CPA treatment. **B.** Anti-P450 2B11 Western blot of microsomal protein extracts prepared from frozen tumor samples after 0–12 days of metronomic CPA treatment. Expression of P450 2B11 protein decreased following the second CPA injection. By day 12, tumor samples showed little or no detectable P450 2B11 protein (last 3 lanes on right).

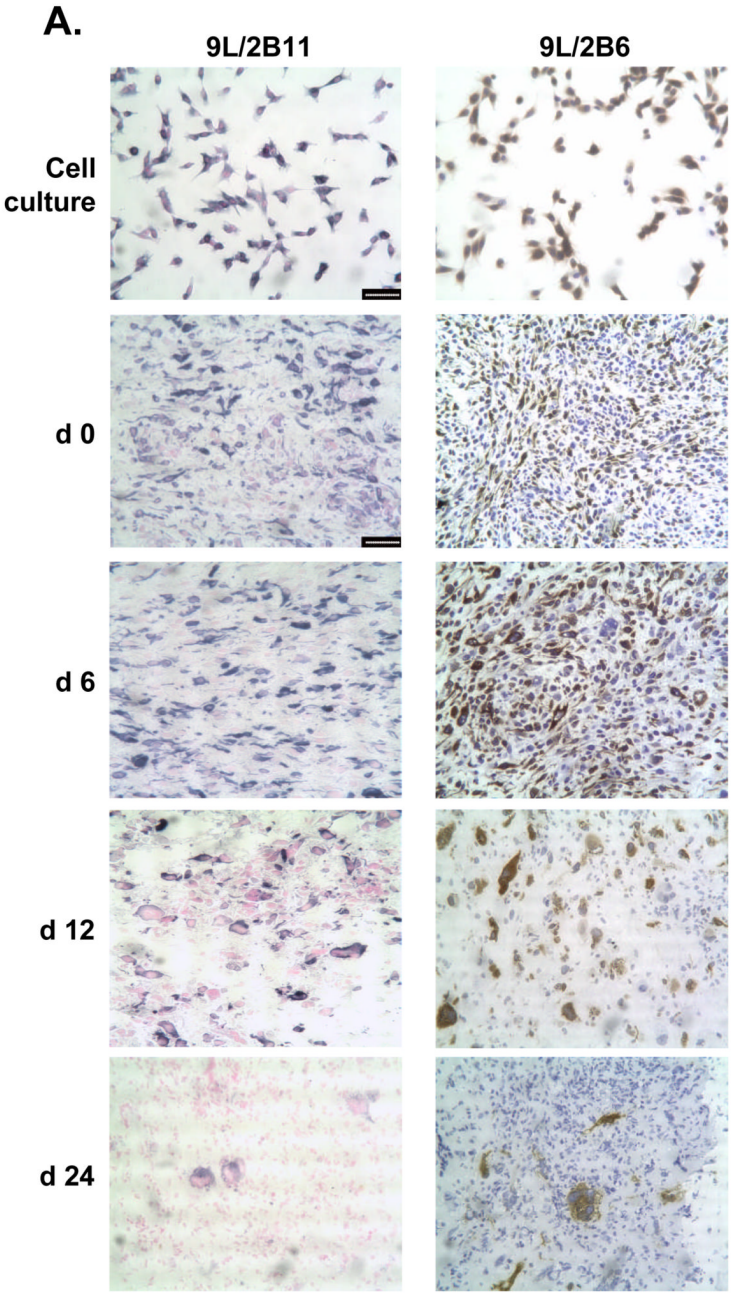

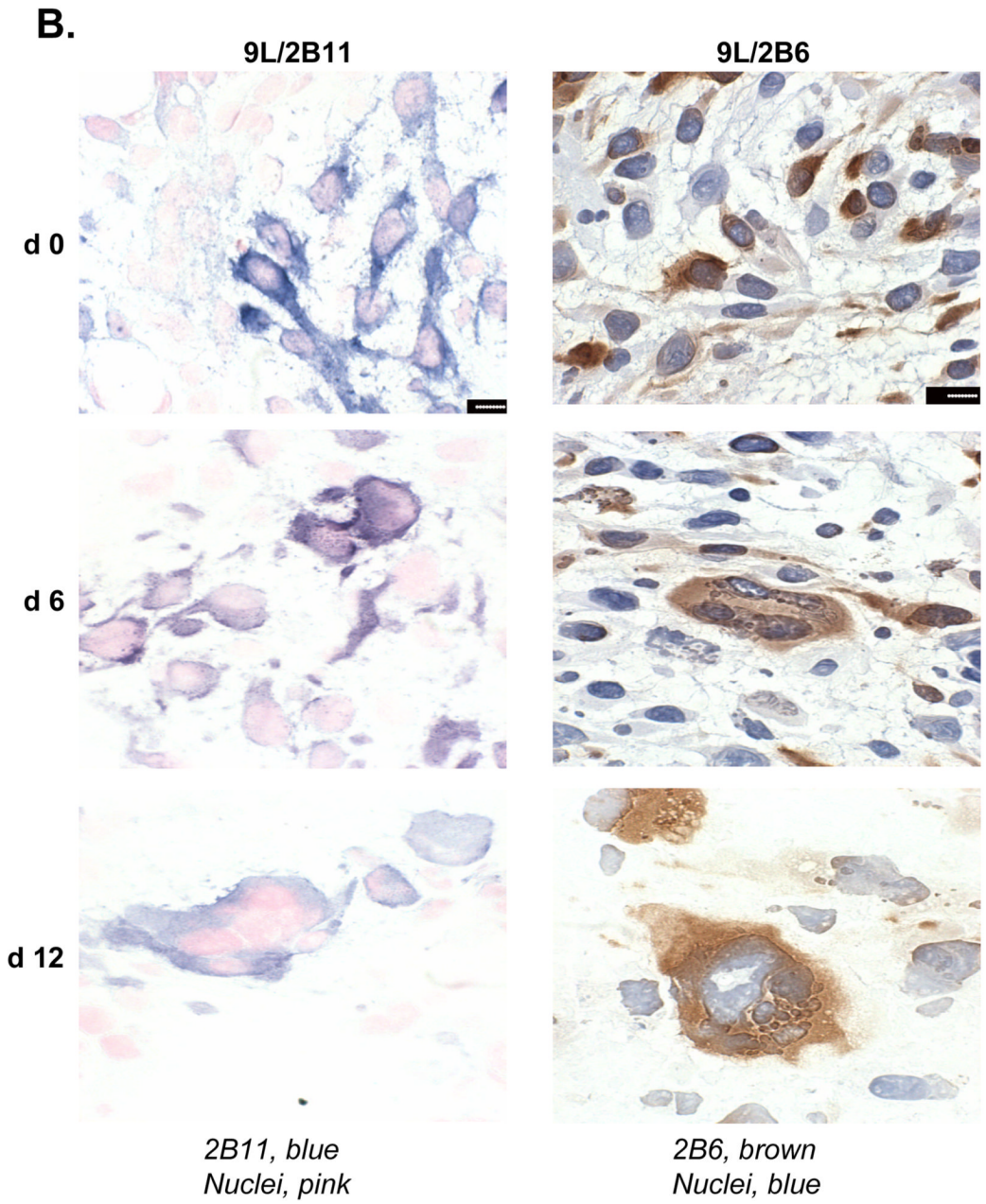

Figure 6. Reduced population of P450-positive cells and their morphological changes in 9L tumors

A. Left panels, cultured 9L/2B11 cells ('cell culture') and 9L/2B11 tumor cryosections (day 0–24 after the first metronomic CPA injection) were immunostained with anti-P450 2B11 antibody (blue) and cell nuclei were labeled by Nuclear Fast Red (pink). Right panels, the corresponding set of cultured 9L/2B6 cells and 9L/2B6 cryosections were immunostained with anti-P450 2B6 antibody (brown) and cell nuclei were stained with hematoxylin (blue). The number of P450-positive cells decreased during metronomic CPA treatment, with re-population by P450-deficient cells evident on day 24, in particular in the case of the 9L/2B6 tumors. Scale bar, 50 μm. **B.** High magnification photos show enlarged P450 2B11 (left) and P450 2B6 (right) positive cells in sections of CPA-treated 9L/2B11 and 9L/2B6 tumors,

respectively. These enlarged cells first appeared on day 6. Untreated tumor cells (day 0) are of normal size. Scale bar, 10 μm.